

Article

# Metal–Organic Framework Fe-BTC as Heterogeneous Catalyst for Electro-Fenton Treatment of Tetracycline

Taylor Mackenzie Fisher , Alessandro J. dos Santos  and Sergi Garcia-Segura \* 

School of Sustainable Engineering and the Built Environment, Arizona State University, Tempe, AZ 85287-3005, USA; tmfishe6@asu.edu (T.M.F.); adossan4@asu.edu (A.J.d.S.)

\* Correspondence: sgarcias@asu.edu

**Abstract:** This study explores the use of the iron-containing metal–organic framework (MOF), Basolite®F300, as a heterogeneous catalyst for electrochemically-driven Fenton processes. Electrochemical advanced oxidation processes (EAOPs) have shown promise on the abatement of recalcitrant organic pollutants such as pharmaceuticals. Tetracyclines (TC) are a frequently used class of antibiotics that are now polluting surface water and groundwater sources worldwide. Acknowledging the fast capability of EAOPs to treat persistent pharmaceutical pollutants, we propose an electrochemical Fenton treatment process that is catalyzed by the use of a commercially available MOF material to degrade TC. The efficiency of H<sub>2</sub>O<sub>2</sub> generation in the IrO<sub>2</sub>/carbon felt setup is highlighted. However, electrochemical oxidation with H<sub>2</sub>O<sub>2</sub> production (ECO-H<sub>2</sub>O<sub>2</sub>) alone is not enough to achieve complete TC removal, attributed to the formation of weak oxidant species. Incorporating Basolite®F300 in the heterogeneous electro-Fenton (HEF) process results in complete TC removal within 40 min, showcasing its efficacy. Additionally, this study explores the effect of varying MOF concentrations, indicating optimal removal rates at 100 mg L<sup>-1</sup> due to a balance of kinetics and limitation of active sites of the catalysts. Furthermore, the impact of the applied current on TC removal is investigated, revealing a proportional relationship between current and removal rates. The analysis of energy efficiency emphasizes 50 mA as the optimal current, however, balancing removal efficiency with electrical energy consumption. This work highlights the potential of Basolite®F300 as an effective catalyst in the HEF process for pollutant abatement, providing valuable insights into optimizing electrified water treatment applications with MOF nanomaterials to treat organic pollutants.

**Keywords:** MOF; electrochemical advanced oxidation processes; heterogeneous Fenton; antibiotics



**Citation:** Fisher, T.M.; dos Santos, A.J.; Garcia-Segura, S. Metal–Organic Framework Fe-BTC as Heterogeneous Catalyst for Electro-Fenton Treatment of Tetracycline. *Catalysts* **2024**, *14*, 314. <https://doi.org/10.3390/catal14050314>

Academic Editor: Hideyuki Katsumata

Received: 10 April 2024

Revised: 28 April 2024

Accepted: 7 May 2024

Published: 10 May 2024



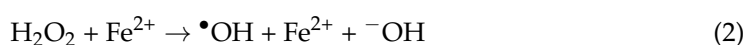
**Copyright:** © 2024 by the authors. Licensee MDPI, Basel, Switzerland. This article is an open access article distributed under the terms and conditions of the Creative Commons Attribution (CC BY) license (<https://creativecommons.org/licenses/by/4.0/>).

## 1. Introduction

Antibiotics are one of the most commonly used pharmaceuticals worldwide to prevent bacterial infections in both humans and animals. One particular group of antibiotics, tetracyclines (TC), represent the highest percentage of antibiotics used due to their relatively low cost and varied application for infections such as gastrointestinal infections, pneumonia, and sexually transmitted infections [1,2]. Despite their popularity in treating a wide range of conditions, these organic compounds do not degrade easily after use due to their composition of various methyl, keto, and diethylamino functional groups [3]. Inefficient removal of TCs during the wastewater treatment process combined with excessive use is resulting in frequent pollution of surface water and groundwater systems [4]. As such, it is essential to research treatment processes aimed at degrading TC in aqueous systems to mitigate the harmful impacts of pharmaceutical pollution posed at both humanity and aquatic ecosystems.

Electrochemical advanced oxidation processes (EAOPs) are emerging as one of the newer environmental technologies to quickly degrade such organic pollutants in water. These processes work by implementing electrochemically-driven reactions to generate strong oxidants in situ such as hydroxyl radicals ( $\bullet\text{OH}$ ). The  $\bullet\text{OH}$  is the second strongest

known oxidant after fluorine with a standard reduction potential of 2.8 V vs. SHE [5]. Electrogenerated  $\bullet\text{OH}$  reacts non-selectively with organics attaining their complete mineralization [6–8]. The EAOPs are performed at standard pressure and room temperature while utilizing electrons as a “cleaner and sustainable agent” instead of a chemical addition [9]. Among EAOPs, the electro-Fenton (EF) process emerges as a highly competitive approach given the high efficiency of indirect  $\bullet\text{OH}$  generation. In EF, the  $\text{H}_2\text{O}_2$  is electrogenerated at a carbonaceous cathode in the presence of Air/ $\text{O}_2$  according to reaction (1). Then  $\bullet\text{OH}$  is produced from the catalytic decomposition of  $\text{H}_2\text{O}_2$  by a redox mediator (e.g.,  $\text{Fe}^{2+}$ ) following Fenton’s reaction (2) [10]. The major limitation of the EF process is the narrow pH window of applicability defined between 3.0 and 4.0, given the precipitation of the catalyst  $\text{Fe}^{2+}/\text{Fe}^{3+}$ . Heterogeneous Fe catalysts hold the promise of enabling a wider range of applicability beyond acidic conditions. Furthermore, heterogeneous catalysts possess a higher rate of reusability [11].



Metal–organic frameworks (MOFs) are an emerging class of nanomaterials composed of metal ions coordinated to organic linkers. These materials self-assemble into crystalline frameworks with extremely high porosity and surface area that is advantageous for nanomaterial engineering in varied industries such as drug delivery, gas storage and separation, and environmental remediation applications [12–14]. Within environmental research, MOFs have been specifically studied for photo-Fenton (PF) degradation of organic water pollutants [15,16] or MOF-derived electro-Fenton degradation of antibiotics [17–20]. However, there is limited research regarding MOF’s direct catalytic potential in heterogeneous electro-Fenton (HEF) applications despite the existence of Fe MOFs such as MIL-53 that have been utilized to degrade antibiotic pollutants [21,22]. Coupled with this knowledge gap is the impediment of MOF’s often complicated synthesis methods that has slowed the upscaling of certain MOF materials from academia onto the industrial market in comparison with other nanomaterials [23]. Identifying the potential to understand how Fe MOFs function within organic pollutant degradation while also acknowledging commercial limitations, this research examines the heterogeneous catalytic potential of Fe-BTC MOF, commercially available as Basolite<sup>®</sup>F300 to remove TC from water via an electrochemical Fenton process.

## 2. Results and Discussion

### 2.1. Material Characterization

Figure 1a shows the characteristic XRD patterns of a semi-crystalline Basolite<sup>®</sup>F300 material. Broad peaks occur most notably at  $2\theta = 11, 14, 19,$  and  $24^\circ$ , and are consistent with the peaks identified in literature of synthesized Fe-BTC MOF [24,25]. Figure 1b illustrates the nitrogen adsorption desorption isotherms of Basolite<sup>®</sup>F300 with a shape characteristic of a mesoporous material with a type IV isotherm [26]. The pore size distribution using the Barrett–Joyner–Halenda (BJH) model was found to be between 2–100 nm with an average pore width of 2.68 nm, and a cumulative pore volume of  $0.39 \text{ cm}^3 \text{ g}^{-1}$ . The average pore width demonstrates a dominance of smaller mesopores and falls within the 2–50 nm range, confirming the mesoporous nature of the Basolite<sup>®</sup>F300 material [26]. Additionally, the material demonstrated a high BET surface area of  $1465 \text{ m}^2/\text{g}$  falling near reported ranges of  $800\text{--}1400 \text{ m}^2/\text{g}$  for either Basolite<sup>®</sup>F300 or various synthesized Fe-BTC material [24,27–29]. It has also been reported by manufacturers that the Basolite<sup>®</sup>F300 surface area is expected to fall within a higher surface area range of  $1300\text{--}1600 \text{ m}^2/\text{g}$  [30].

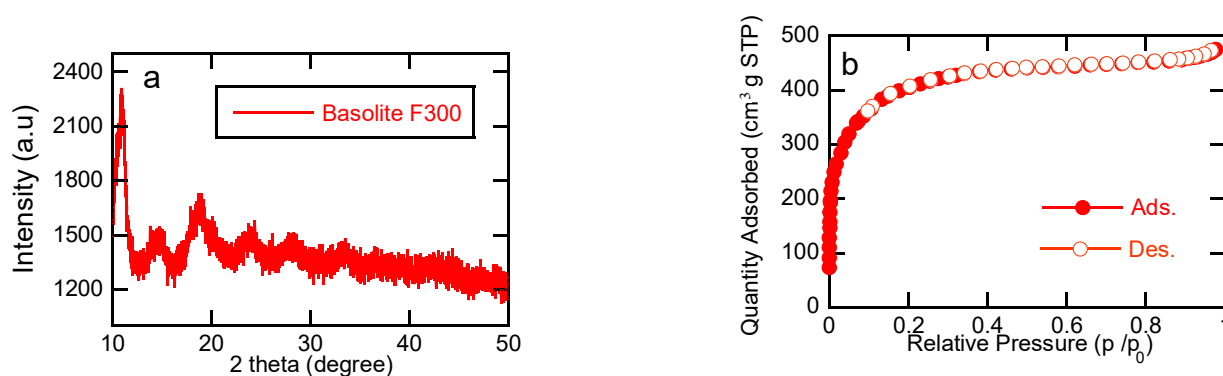
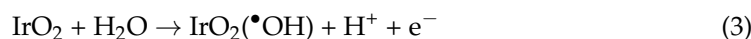


**Figure 1.** (a) XRD Spectra (b) N<sub>2</sub> adsorption-desorption isotherm data of the Basolite<sup>®</sup>F300 material.

## 2.2. Degradation of TC by Electrochemical Methods

Initially, the capacity of the lab-scale cell to generate and accumulate H<sub>2</sub>O<sub>2</sub> was investigated using an IrO<sub>2</sub>/carbon felt setup under electrochemical oxidation in the presence of H<sub>2</sub>O<sub>2</sub> (ECO-H<sub>2</sub>O<sub>2</sub>) conditions. This experiment employed 50 mM Na<sub>2</sub>SO<sub>4</sub> as the supporting electrolyte at a pH of 7.0 and applied a current of 50 mA. As illustrated in Figure 2a, the progressive accumulation of H<sub>2</sub>O<sub>2</sub> reached a final concentration of 14.1 mg L<sup>-1</sup> after 60 min of electrolysis. The formation of H<sub>2</sub>O<sub>2</sub> through the electrocatalytic 2e<sup>-</sup> oxygen reduction reaction (ORR) by reaction (1) is well discussed in the literature [31–34]. The amount of electrogenerated H<sub>2</sub>O<sub>2</sub> accumulated is sufficient for facilitating the Fenton’s reaction, given the traditional use of low H<sub>2</sub>O<sub>2</sub> concentrations in classical Fenton systems. Additionally, the electrochemical system continuously produces H<sub>2</sub>O<sub>2</sub> in situ, ensuring that this reagent does not become the limiting factor for Fenton’s reaction. Then, for comparative analysis, a synthetic effluent containing 10 mg L<sup>-1</sup> of TC was submitted to treatment under blank conditions of ECO-H<sub>2</sub>O<sub>2</sub> and adsorption without a supply of electrical current. Figure 2b illustrates the percentage of TC removal over time, showing a limited removal of the pollutant under both employed conditions. After 60 min, only 10% of TC was removed by ECO-H<sub>2</sub>O<sub>2</sub> via the system set up with no MOF catalyst present. This result indicated that the IrO<sub>2</sub> anode had minimal electrocatalytic activity for TC degradation. Although IrO<sub>2</sub> can generate hydroxyl radicals from water oxidation following reaction (3), those are stabilized on the electrode surface as chemisorbed superoxides following reaction (4) [35]. The IrO<sub>3</sub> superoxide is a weak oxidant that is unable to efficiently oxidize TC leading to only partial oxidation as described by reaction (5) [36]. This characteristic makes IrO<sub>2</sub> an active anode material, however, it is still commonly utilized in electrified technologies due to its low cost compared to other electrocatalytic materials such as boron-doped diamond (BDD) [37–39]. In consideration of the cost of the MOF catalyst, it is important that the electrochemical system also be cost-effective, and thus DSA IrO<sub>2</sub> was utilized instead of BDD.



Electroanalytical experiments conducted in the presence and absence of TC (Figure 2c) demonstrate the absence of direct electron transfer mechanisms for TC oxidation during cyclic voltammetry (CV) analyses. This is seen in the absence of oxidation peaks before the onset of oxygen evolution reaction (OER). It is worth noting, however, that the electrogenerated H<sub>2</sub>O<sub>2</sub> does not contribute to degradation due to its high stability in solution and its lower oxidation potential ( $E^\circ = 1.78$  V vs. SHE) [5]. Therefore, we conclude that the 10% removal observed in the ECO-H<sub>2</sub>O<sub>2</sub> process is primarily due to the incomplete removal of TC by superoxides. Regarding adsorption, 20.2% TC removal is achieved, slightly higher than ECO-H<sub>2</sub>O<sub>2</sub> removal due to the highly porous structure of Basolite<sup>®</sup>F300 with a large

surface area that is advantageous for adsorption. Increasing the rate of adsorption capacity of Basolite® F300 for TC pollutants would likely require a larger amount of MOF material and that is not advantageous for the application of this material due to cost.

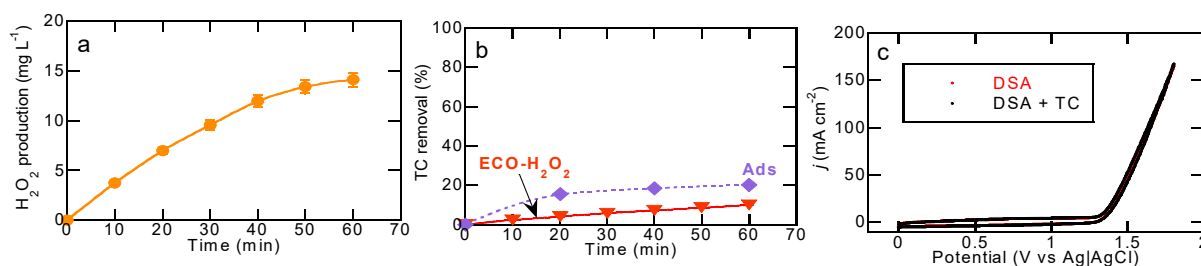


**Figure 2.** (a) H<sub>2</sub>O<sub>2</sub> production rate; (b) TC removal achieved by ECO-H<sub>2</sub>O<sub>2</sub> and adsorption processes; (c) CV analysis of the electrochemical system.

The use of iron-based MOFs can be potentially exploited as heterogeneous catalysts for the Fenton reaction. Figure 3a demonstrates that the addition of the MOF to the solution to conduct a heterogeneous electro-Fenton process (HEF) resulted in complete pollutant removal within just 40 min of electrolysis. Furthermore, a comparative homogeneous EF process was tested using 0.03 mM Fe<sup>2+</sup>, a concentration similar to that leached from the MOF (Appendix A). The homogeneous EF driven by reaction (2) contributed to a lower percentage of TC degradation, achieving only 48% removal. This limitation is attributed to the lower availability of Fe<sup>2+</sup> ions, where the leached concentration from the MOF is more than 10 times lower than the typical Fe<sup>2+</sup> concentration in homogeneous EF processes. This result suggests that the HEF is mostly driven by heterogeneous activation of H<sub>2</sub>O<sub>2</sub> and not by iron leached to the solution. In Figure 3b, the pseudo-first-order rate constant (*k*<sub>1</sub>) values are presented, showing an increasing order of ECO-H<sub>2</sub>O<sub>2</sub> ( $1.8 \times 10^{-3} \text{ min}^{-1}$  R<sup>2</sup> = 0.996), EF ( $1.2 \times 10^{-2} \text{ min}^{-1}$  R<sup>2</sup> = 0.991), and HEF ( $8.4 \times 10^{-2} \text{ min}^{-1}$  R<sup>2</sup> = 0.993). This represents a 46-fold increase from the process with the lowest TC degradation to the highest. The behavior observed is dependent on the oxidative power of each process, where HEF predominates the degradation kinetics at 86%, complemented by a discrete 14% from homogeneous reactions that also contributed to hydroxyl radical formation. These data demonstrate that the main degradation route of TC is through the generation of free radicals formed from heterogeneous Fenton-like reactions between the Fe<sup>3+</sup> of Basolite® F300 and H<sub>2</sub>O<sub>2</sub> at the catalyst surface described by reaction (6). The reduction in ≡Fe<sup>3+</sup> induced by a Fenton-like reaction (7) results in the regeneration of ≡Fe<sup>2+</sup> that reacts with hydrogen peroxide to form hydroxyl radicals in an ongoing heterogeneous redox cycle that contributes to an overall degradation of TC [40,41].

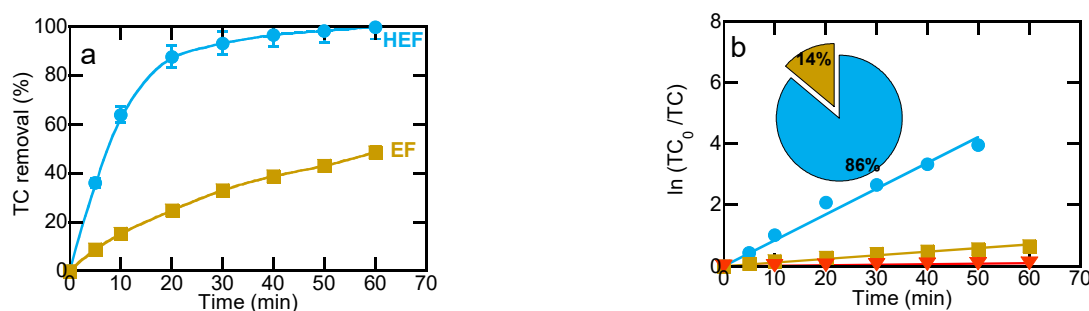
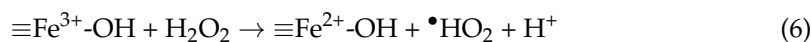


**Figure 3.** (a) TC removal percentage achieved by HEF and EF reactions; (b) kinetic removal rates achieved by (●) HEF, (■) EF, and (▼) ECO-H<sub>2</sub>O<sub>2</sub> processes.

### 2.3. Effect of MOF Dose on Heterogeneous Electro-Fenton Performance

One crucial aspect of HEF treatment revolves around determining the optimal catalyst dosage to achieve swift removal while minimizing the amount of catalyst required, thereby reducing operational costs. In this context, the catalyst dosage was examined across a range of MOF concentrations from 25 to 200 mg L<sup>-1</sup> for the treatment of solutions containing 10 mg L<sup>-1</sup> of TC at pH 6.5. This evaluation was performed while maintaining a consistent solution volume of 100 mL and an applied current of 50 mA. As the MOF dose was increased in the HEF system, the rate of TC removal increased significantly (see Figure 4a). The first-order kinetic rate of removal increased as the dose was increased, with the kinetic change most drastic from 50 mg L<sup>-1</sup> to 100 mg L<sup>-1</sup> as the rate more than doubled from 0.035 min<sup>-1</sup> to 0.082 min<sup>-1</sup> (Figure 4b). The faster removal of TC as the MOF concentration increased can be attributed to the promotion of heterogeneous Fenton reactions as the amount of Fe catalytic sites to promote reaction (6) increased [42]. More notable, however, is the negligible increase in kinetic rate when the MOF dose doubled from 100 to 200 mg L<sup>-1</sup> in Figure 4b from 0.082 min<sup>-1</sup> to 0.111 min<sup>-1</sup>. When dosing Basolite<sup>®</sup>F300 at 100 and 200 mg L<sup>-1</sup>, 95–100% TC removal was also achieved for both concentrations around 40 min. Increasing the dose of Basolite<sup>®</sup>F300 may also have impacts on the adsorptive removal of TC. Figure 4c depicts the percentage of TC removal that occurred via adsorption for each concentration. An increased percentage of physical removal by adsorption reaching 36.5% is observed when increasing the MOF dose to 200 mg L<sup>-1</sup>. However, the faster removal rate observed for HEF demonstrates the driving mechanism of TC abatement. Furthermore, the adsorption of TC close to the catalytic sites that drive the Fenton-like reaction (6) can contribute to overcoming mass transfer limitations on the treatment of trace pollutants following a targeted pollutant trap and zap mechanism [43]. When considering synergies among all of these factors, it becomes apparent that the most advantageous choice for HEF removal is the concentration of 100 mg L<sup>-1</sup> of Basolite<sup>®</sup>F300, exhibiting fast kinetics dominated by Fenton reactions, but also achieving nearly the same 100% removal time as larger catalyst doses. To the best of our knowledge, the results achieved by utilizing a 100 mg L<sup>-1</sup> dose of Basolite<sup>®</sup>F300 in this study are highly competitive when compared to other heterogeneous catalysts that have been previously researched. This work was compared to previous studies that tested the insertion of heterogeneous catalysts directly in solution to catalyze the degradation of TC at various doses in Table 1 [44–49]. When considering the catalyst dose, degradation time, and the facile synthesis of the already commercially available material, it becomes evident that this study shows that the use of Basolite<sup>®</sup>F300 is most advantageous. Despite considering the relatively low cost of the MOF Basolite<sup>®</sup>F300 of \$30.40 per gram (Sigma Aldrich, St. Louis, MO, USA) when compared with other custom MOF materials and the reusability of the heterogeneous catalyst, maximizing treatment performance while minimizing catalyst dosage would be key to ensure a translative application of HEF processes.

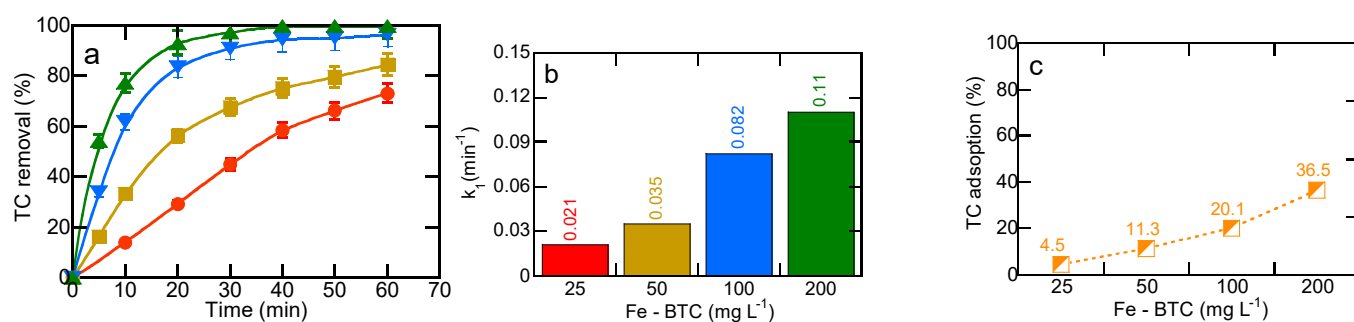


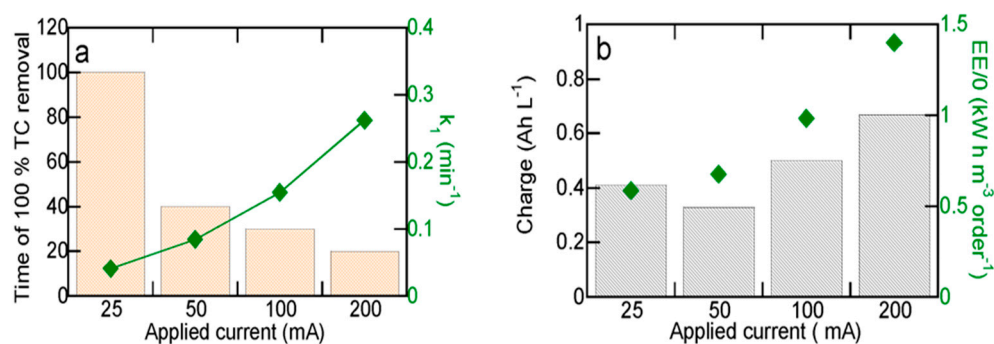
**Figure 4.** (a) Impact of different MOF dosing on TC removal through HEF and (b) corresponding kinetic removal rates. (c) Blank experiments to assess percent of TC removal achieved by only adsorption processes. MOF dose: (●) 25 mg L<sup>-1</sup>, (■) 50 mg L<sup>-1</sup>, (▼) 100 mg L<sup>-1</sup>, (▲) 200 mg L<sup>-1</sup>.

**Table 1.** Comparison of different heterogeneous catalytic materials to degrade TC via electrochemical Fenton reaction.

Catalyst Material	Catalyst Conc.	TC Conc.	Percent Degradation	Time to Achieve Removal	Reference
Fe-BTC Basolite®F300	100 mg L <sup>-1</sup>	10 mg L <sup>-1</sup>	100%	40 min	This publication
Fe <sub>3</sub> O <sub>4</sub> nanoparticles	200 mg L <sup>-1</sup>	25 mg L <sup>-1</sup>	86.53%	60 min	[44]
Synthetic ilmenite (FeTiO <sub>3</sub> ) nanoparticles	15 mg L <sup>-1</sup>	10 mg L <sup>-1</sup>	61.4%	120 min	[45]
Core-shell Fe@Fe <sub>2</sub> O <sub>3</sub> -CeO <sub>2</sub>	80 mg L <sup>-1</sup>	50 mg L <sup>-1</sup>	90.7%	60 min	[46]
Microbial cellulose/Fe <sub>3</sub> O <sub>4</sub> nanocomposite	500 mg L <sup>-1</sup>	50 mg L <sup>-1</sup>	100%	20 min	[47]
Chalcopyrite	1000 mg L <sup>-1</sup>	89 mg L <sup>-1</sup>	86%	120 min	[48]
Graphitic carbon nitride nanosheets decorated with Fe <sub>3</sub> O <sub>4</sub>	20 mg L <sup>-1</sup>	10 mg L <sup>-1</sup>	90%	60 min	[49]

#### 2.4. Effect of Applied Current as Key Parameter of Electrochemically-Driven Technologies

The applied current is a key operational variable in the electrocatalytic process since it defines the amount of electrons delivered to the system per unit of time, therefore controlling the kinetics of reactions [50,51]. In the case of HEF, the applied current defines the kinetics of the electrogeneration of H<sub>2</sub>O<sub>2</sub> and the overall Faradaic efficiency of the process. To determine the optimal applied current to run the HEF reaction, applied currents from 25 mA up to 200 mA were evaluated as depicted in Figure 5a. With an increase in the applied current, the time to achieve 100% TC removal was decreased from 100 min at the lowest current to just 20 min at the highest current. The improvement in TC degradation kinetics can be explained by the greater amount of •OH generated by Equations (5) and (6), given the larger availability of electrogenerated H<sub>2</sub>O<sub>2</sub>.

**Figure 5.** Impacts of applied current on (a) time length (min) to achieve complete TC removal versus kinetic values and (b) charge versus electrical energy per order.

The  $k_1$  data supports this observation, as the  $k_1$  values align well with pseudo-first-order kinetics in ascending order: 0.041 min<sup>-1</sup>, 0.084 min<sup>-1</sup>, 0.155 min<sup>-1</sup>, and 0.272 min<sup>-1</sup> for currents of 25, 50, 100, and 200 mA, respectively (Figure 5a). However, it is important to recognize that selecting the optimal current based solely on electrolysis time may not suffice, as it overlooks energy efficiency considerations. For a more comprehensive assessment of process efficiency, the relationship between the applied electrical charge ( $Q$ ) and applied current is presented in Figure 5b. Notably, transitioning from 25 mA to 50 mA resulted in a decrease in  $Q$ . This reduction can be attributed to the difficulty of 25 mA to generate sufficient H<sub>2</sub>O<sub>2</sub>, thereby compromising the performance of the Fenton reaction. Conversely, surpassing 50 mA led to an increase in  $Q$ . From these observations, two key conclusions

were drawn: (i) 50 mA emerges as the optimal current for the system, as it yielded the lowest  $Q$  value for a given removal percentage of TC; (ii) currents above 50 mA exhibit an increase in  $Q$  due to heightened cell potential. Note that although the production of  $H_2O_2$  increases as the current increases, this reagent instability in solution can be disadvantageous towards the oxidation of the anode surface [52]. Additionally, elevated current levels promote the 4-electron pathway, wherein oxygen ( $O_2$ ) undergoes reduction to form water as competitive reaction (8) that decreases overall efficiency [53]. Furthermore, an excess of  $H_2O_2$  can consume produced  $\bullet OH$  according to parasitic reaction (9), yielding weaker oxidant hydroperoxyl radical ( $HO_2\bullet$ ).



Lastly, we delve into the assessment of energy consumption per order ( $EE/O$ ), calculated using Equation (10). Here,  $E_{cell}$  represents the average cell potential,  $I$  denotes current intensity,  $t$  signifies time (h),  $V_s$  reflects solution volume (in L), and  $C_0$  and  $C_t$  denote initial and final concentrations, respectively. The  $EE/O$  signifies the electrical energy needed to reduce the concentration of a target contaminant by 90%, i.e., by one order of magnitude. This metric is particularly relevant for treatment scenarios following pseudo-first-order kinetics, typical in many electrified applications for water treatment. The  $EE/O$  values for 25 mA and 50 mA remain relatively constant at 0.58 and 0.67 kWh m<sup>-3</sup> order<sup>-1</sup>, respectively, followed by an increase to 0.98 and 1.14 kWh m<sup>-3</sup> order<sup>-1</sup> for 100 mA and 200 mA. Considering all these results, the choice of 50 mA emerges as the most plausible, as it yields not only a lower  $Q$  value, but also a correspondingly low  $EE/O$  value.

$$EE/O(\text{kWh m}^{-3} \text{ order}^{-1}) = \frac{E_{cell}It}{V_s \log(C_0/C_t)} \quad (10)$$

### 3. Experimental Section

#### 3.1. Chemicals

All chemicals utilized for preparation and analysis were of analytical grade supplied by Sigma Aldrich (St. Louis, MO, USA) and employed without further modification. This includes MOF Fe-BTC, denoted as Basolite<sup>®</sup>F300, and TC (CAS 60-54-8, 99%). The physicochemical characteristics of TC are detailed below in Table 2 [54,55]. Sodium sulfate served as the supporting electrolyte, while iron (II) sulfate heptahydrate was utilized for homogeneous Fenton reactions. Titanium (IV) oxysulfate played a role in quantifying the produced hydrogen peroxide, and sulfuric acid was used for activating the carbon felt. All solutions were freshly prepared using ultrapure water from the Elga Lab system.

**Table 2.** Characteristics of tetracycline.

Compound	Molecular Weight (g/mol)	Molecular Formula	Solubility (mol/L)	P <sub>kw</sub>	P <sub>ka1</sub>	P <sub>ka2</sub>
Tetracycline	444.44	C <sub>22</sub> H <sub>24</sub> N <sub>2</sub> O <sub>8</sub>	0.041	−1.25	3.2	7.78

#### 3.2. Characterization Techniques

Basolite<sup>®</sup>F300 was characterized via powder X-ray diffraction using a Panalytical Aeris powder X-ray diffractometer (Malvern Panalytical, Malvern, UK). The spectra were collected from 10 to 50° with a resolution of 0.01. Nitrogen adsorption–desorption analysis using the Brunauer–Emmett–Teller (BET) theory was performed on the Tristar II 3020 (Micromeritics Instrument Corporation, Norcross, GA, USA) to obtain the BET surface area. Prior to analysis, the samples were degassed overnight for 12 h at 150 °C [27].

### 3.3. Electrochemical Setup

The experiments were conducted on a lab-scale electrochemical cell equipped with a DSA<sup>®</sup> (IrO<sub>2</sub>) anode obtained from De Nora (Milan, Italy) and a carbon felt (CF) cathode purchased from Fuel Cell Store (College Station, TX, USA). Before use, the cathode underwent activation using a 40% sulfuric acid solution for 8 h, followed by thorough cleaning and sonication with ultrapure water for an additional 2 h. To ensure optimal conditions, the solution was saturated with pure O<sub>2</sub> at a rate of 0.3 L min<sup>-1</sup> to facilitate H<sub>2</sub>O<sub>2</sub> electrogenerated. The experiments were performed at least in duplicate under a galvanostatic mode utilizing the TENMA 72-2720 DC power supply. Three different EAOPs were assessed in this study: electrochemical oxidation with hydrogen peroxide electrogeneration (ECO-H<sub>2</sub>O<sub>2</sub>), homogeneous electro-Fenton (EF), and heterogeneous electro-Fenton (HEF). For HEF, the impacts of catalyst concentration (25–200 mg L<sup>-1</sup>) and applied current (25–200 mA) were investigated. The suspension was continuously stirred for 20 min to achieve adsorption–desorption equilibrium before operating the system galvanostatically. ECO-H<sub>2</sub>O<sub>2</sub> and HEF experiments were conducted at a pH of 6.5, which is representative of the natural TC pH, stirred at 200 rpm, and maintained at room temperature (Figure 6). In contrast, the EF experiment was carried out at a pH of 3.0 to prevent the precipitation of iron oxyhydroxides.

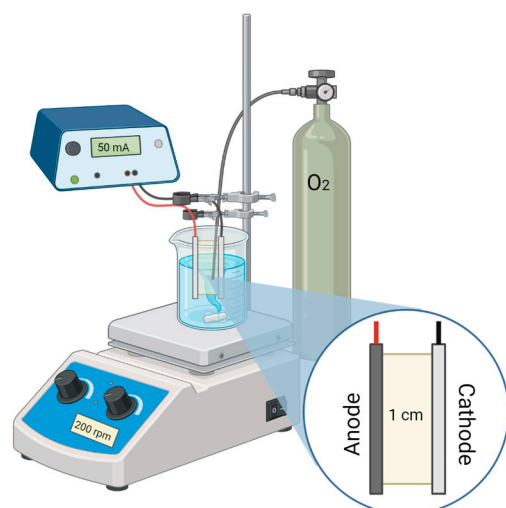


**Figure 6.** Electrochemical experimental setup.

### 3.4. Analytical Techniques

The total amount of Fe leached in the system was quantified via inductively coupled plasma mass spectroscopy (ICP-MS). ICP-MS measurements were performed on a NexIon 1000 mass spectrometer (PerkinElmer, Waltham, MA, USA) run in helium KeV mode for Fe interferences. Standards were prepared and used at 10, 25, 50, 100, 250, and 500 parts per million (ppm) concentrations with an  $R^2 = 0.999$ . Samples were specifically tested for Fe 56 isotope, the most abundant type of Fe isotope. Next, the dissolved Fe<sup>2+</sup> concentration in the solution was measured via ultraviolet-visible (UV-vis) absorption on a DR6000 UV-vis spectrophotometer (Hach, Ames, IA, USA). Samples were measured for adsorption of dissolved Fe<sup>2+</sup> after 10 min of complexation with a 1,10-phenanthroline compound and at maximum absorbance  $\lambda = 510$  nanometers (nm). The amount of Fe<sup>2+</sup> concentration was subtracted from the total Fe concentration measured to determine the amount of Fe<sup>3+</sup> remaining in the solution after 60 min of EF reaction. Hydrogen peroxide was quantified utilizing the Ti(IV)-complex method, and absorbance measurements were recorded at a maximum wavelength of 408 nm. High-performance liquid chromatography (HPLC) was used to determine the amount of TC remaining in the solution over time. We utilized the Waters HPLC model e2695 in conjunction with a C-18 column (75 mm  $\times$  4.6 mm, 3.5  $\mu$ m) coupled with a PDA detector set to monitor at 358 nm. For chromatographic separation,

we employed a mobile phase, composed of a 40:60 blend of acetonitrile and phosphoric acid, operating at a flow rate of 0.2 mL min<sup>-1</sup>. Cyclic voltammetry (CV) was used to evaluate the electrochemical response of the catalytic system. Potentiostatic measurements were performed using a three-electrode system, consisting of IrO<sub>2</sub> as a working electrode, stainless steel as a counter-electrode, and Ag/AgCl (~3 mol L<sup>-1</sup> KCl) as the reference electrode. The CV analyses were conducted in 50 mM sulfuric acid solution using the Autolab PG302N machine (Metrohm, Herisau, Switzerland) in a potential range of 0 to 1.8 V vs. Ag/AgCl at a scan rate of 50 mV s<sup>-1</sup>.

#### 4. Conclusions

This present work demonstrates that the commercially available Fe-BTC MOF, known as Basolite®F300, can be applied as a heterogeneous catalyst to degrade tetracycline (TC) antibiotics in water. Emerging Fe-MOFs have been recently studied for photocatalytic treatment and adsorption but have barely been explored in electrochemical water treatment processes. The MOF materials possess highly catalytic and adsorptive capabilities that may be advantageous for research within water treatment processes. With these considerations, a low-cost Fe-MOF was used as a heterogeneous catalyst for the electro-Fenton treatment of TC. Results showcase the heterogeneous nature of the process that attained complete TC removal after 40 min of treatment. Heterogeneous TC removal was achieved at a significantly more rapid rate than removal via traditional homogeneous Fenton reactions, adsorption, or electrochemical oxidation with no MOF catalyst. Examination of key experimental variables further revealed that an optimal catalyst concentration of up to 100 mg maximizes TC removal efficiency. Beyond this value, no substantial improvement was observed, likely due to an excess of active sites in the catalyst remaining unutilized. Additionally, higher applied currents exhibited fast pollutant removal, evidenced by increased  $k_1$  values. However, increasing currents above the optimal chosen current of 50 mA resulted in higher EEO values, indicating a reduced efficiency relative to the associated electrical charge ( $Q$ ). The use of F-MOF in this study provides insight into how MOF materials can be used to improve EAOPs that are now identified as a fast and more sustainable way to treat emerging pharmaceutical pollutants. This work reveals the capability of direct application of MOF material, not just MOF-derived nanomaterials, to directly and effectively catalyze the degradation of antibiotic contaminants in electrochemically-driven treatments. This MOF material, along with similar Fe-based MOFs, could be implemented in other electrocatalytic treatment processes or to degrade other pollutants of interest, as well as to activate stronger oxidants. Further studies should be performed, however, to assess its cost-effectiveness in comparison with other catalysts used in EAOPs, water stability, and life cycle reuse. One of the major challenges of nanoparticulated catalyst use that may arise as an implementation barrier is the separation from solution after use and/or the possible recovery for reuse. The design of modified electrodes with integrated catalytic MOF materials to overcome possible reuse and recovery concerns is needed.

**Author Contributions:** Conceptualization, T.M.F. and A.J.d.S.; methodology, T.M.F. and A.J.d.S.; validation, T.M.F. and A.J.d.S.; formal analysis, A.J.d.S.; investigation, T.M.F. and A.J.d.S.; resources, T.M.F., A.J.d.S. and S.G.-S.; data curation, A.J.d.S. and T.M.F.; writing—original draft preparation, T.M.F.; writing—review and editing, T.M.F., A.J.d.S. and S.G.-S.; visualization, A.J.d.S. and T.M.F.; supervision, S.G.-S.; project administration, A.J.d.S.; funding acquisition, S.G.-S. All authors have read and agreed to the published version of the manuscript.

**Funding:** The National Science Foundation (NSF) through the Nanosystems Engineering Research Center for Nanotechnology-Enabled Water Treatment (EEC-1449500) and CBET-1708681. T.M.F. also acknowledges the support of Arizona State University through the Dean’s Fellowship as well as NSF through the GRFP fellowship.

**Data Availability Statement:** The original contributions presented in the study are included in the article. Further inquiries can be directed to the corresponding authors.

**Conflicts of Interest:** The authors declare no conflicts of interest.

## Appendix A

A combination of UV-vis and ICP-MS analysis was performed to determine the amount of Fe species released by the Basolite®F300 MOF during HEF experimentation and thus confirmed the dominant Fenton reaction occurring. After 60 min, the total Fe concentration leached from the Basolite®F300 MOF measured via ICP-MS was 2.39 ppm ( $\text{mg L}^{-1}$ ) from an initial MOF concentration of  $100 \text{ mg L}^{-1}$ . When measuring for  $\text{Fe}^{2+}$  concentration via UV-vis analysis, the  $\text{Fe}^{2+}$  concentration was calculated to be 1.87 ppm and as a result, the  $\text{Fe}^{3+}$  concentration was found to be 0.52 ppm. This translates to 78.2% of  $\text{Fe}^{3+}$  in the original MOF structure being converted to  $\text{Fe}^{2+}$  species after 1 h of electrocatalysis, which is concurrent with heterogeneous Fenton-like reactions. This demonstrates the extent to which Basolite®F300 is functioning as a heterogeneous catalyst, where the electrocatalytic mechanism is driven by the redox cycling of coupled  $\text{Fe}^{3+}/\text{Fe}^{2+}$  in the solution [18]. The MOF catalyst transforms to produce predominantly  $\text{Fe}^{2+}$  species that catalyze the decomposition of  $\text{H}_2\text{O}_2$  to produce stronger hydroxyl radicals than those released in Equation (2) [39].

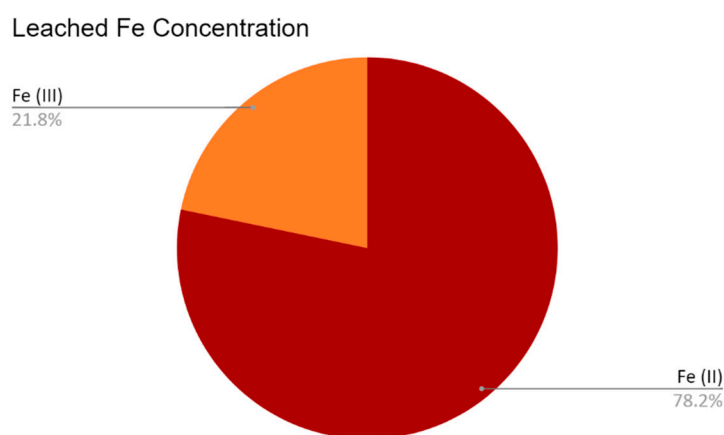


**Figure A1.** Fraction of Fe (II) and Fe (III) compounds remaining after 1 h of HEF removal.

## References

- Amangelsin, Y.; Semenova, Y.; Dadar, M.; Aljofan, M.; Bjørklund, G. The Impact of Tetracycline Pollution on the Aquatic Environment and Removal Strategies. *Antibiotics* **2023**, *12*, 440. [CrossRef]
- Huang, Z.; Wang, H.; Hong, J.; Zhao, L. MOF-derived  $\text{Fe}_2\text{O}_3/\text{C}$ -coupled  $\text{Bi}_2\text{MoO}_6$  heterojunctions for highly efficient Photo-Fenton degradation of tetracycline. *J. Mol. Liq.* **2023**, *383*, 122157. [CrossRef]
- Fiaz, A.; Zhu, D.; Sun, J. Environmental fate of tetracycline antibiotics: Degradation pathway mechanisms, challenges, and perspectives. *Environ. Sci. Eur.* **2021**, *33*, 64. [CrossRef]
- Zhang, F.; Wang, J.; Tian, Y.; Liu, C.; Zhang, S.; Cao, L.; Zhou, Y.; Zhang, S. Effective removal of tetracycline antibiotics from water by magnetic functionalized biochar derived from rice waste. *Environ. Pollut.* **2023**, *330*, 121681. [CrossRef]
- Amor, C.; Marchão, L.; Lucas, M.S.; Peres, J.A. Application of Advanced Oxidation Processes for the Treatment of Recalcitrant Agro-Industrial Wastewater: A Review. *Water* **2019**, *11*, 205. [CrossRef]
- dos Santos, A.J.; Fortunato, G.V.; Kronka, M.S.; Vernasqui, L.G.; Ferreira, N.G.; Lanza MR, V. Electrochemical oxidation of ciprofloxacin in different aqueous matrices using synthesized boron-doped micro and nano-diamond anodes. *Environ. Res.* **2022**, *204*, 112027. [CrossRef] [PubMed]
- Garcia-Segura, S.; Ocon, J.D.; Chong, M.N. Electrochemical oxidation remediation of real wastewater effluents—A review. *Process Saf. Environ.* **2018**, *113*, 48–67. [CrossRef]
- Lu, S.; Liu, L.; Demissie, H.; An, G.; Wang, D. Design and application of metal-organic frameworks and derivatives as heterogeneous Fenton-like catalysts for organic wastewater treatment: A review. *Environ. Int.* **2021**, *146*, 106273. [CrossRef]
- dos Santos, A.J.; Kronka, M.S.; Fortunato, G.V.; Lanza MR, V. Recent advances in electrochemical water technologies for the treatment of antibiotics: A short review. *Curr. Opin. Electrochem.* **2021**, *26*, 100674. [CrossRef]
- Brillas, E.; Sirés, I.; Oturan, M.A. Electro-fenton process and related electrochemical technologies based on fenton's reaction chemistry. *Chem. Rev.* **2009**, *109*, 6570–6631. [CrossRef]
- Nidheesh, P.V.; Olvera-Vargas, H.; Oturan, N.; Oturan, M.A. Heterogeneous electro-Fenton process: Principles and applications. *Handb. Environ. Chem.* **2018**, *61*, 85–110. [CrossRef]
- Lawson, H.D.; Walton, S.P.; Chan, C. Metal-Organic Frameworks for Drug Delivery: A Design Perspective. *ACS Appl. Mater. Interfaces* **2021**, *13*, 7004–7020. [CrossRef]

13. Li, H.; Wang, K.; Sun, Y.; Lollar, C.T.; Li, J.; Zhou, H.C. Recent advances in gas storage and separation using metal–organic frameworks. *Mater. Today* **2018**, *21*, 108–121. [[CrossRef](#)]
14. Ma, Q.; Li, Y.; Tan, Y.; Xu, B.; Cai, J.; Zhang, Y.; Wang, Q.; Wu, Q.; Yang, B.; Huang, J. Recent Advances in Metal-Organic Framework (MOF)-Based Photocatalysts: Design Strategies and Applications in Heavy Metal Control. *Molecules* **2023**, *28*, 6681. [[CrossRef](#)]
15. Mumtaz, N.; Javaid, A.; Imran, M.; Latif, S.; Hussain, N.; Nawaz, S.; Bilal, M. Nanoengineered metal-organic framework for adsorptive and photocatalytic mitigation of pharmaceuticals and pesticide from wastewater. *Environ. Pollut.* **2022**, *308*, 119690. [[CrossRef](#)]
16. Wang, Y.; Zhao, M.; Hou, C.; Chen, W.; Li, S.; Ren, R.K.; Li, Z. Efficient degradation of perfluorooctanoic acid by solar photo-electro-Fenton like system fabricated by MOFs/carbon nanofibers composite membrane. *Chem. Eng. J.* **2021**, *414*, 128940. [[CrossRef](#)]
17. Huang, S.; Wang, Y.; Qiu, S.; Wan, J.; Ma, Y.; Yan, Z.; Xie, Q. In-situ fabrication from MOFs derived Mn<sub>x</sub>Co<sub>3-x</sub>@C modified graphite felt cathode for efficient electro-Fenton degradation of ciprofloxacin. *Appl. Surf. Sci.* **2022**, *586*, 152804. [[CrossRef](#)]
18. Ye, Z.; Padilla, J.A.; Xuriguera, E.; Brillas, E.; Sirés, I. Magnetic MIL(Fe)-type MOF-derived N-doped nano-ZVI@C rods as heterogeneous catalyst for the electro-Fenton degradation of gemfibrozil in a complex aqueous matrix. *Appl. Catal. B Environ.* **2020**, *266*, 118604. [[CrossRef](#)]
19. Zheng, Y.; Du, X.; Song, G.; Gu, J.; Guo, J.; Zhou, M. Degradation of carbamazepine over MOFs derived FeMn@C bimetallic heterogeneous electro-Fenton catalyst. *Chemosphere* **2023**, *312*, 137353. [[CrossRef](#)]
20. Zhou, Y.; Wang, J. Degradation of Cephalosporin C using MOF-derived Fe-Co bimetal in carbon cages as electro-Fenton catalyst at natural pH. *Sep. Purif. Technol.* **2023**, *323*, 124388. [[CrossRef](#)]
21. Du, X.; Fu, W.; Su, P.; Zhang, Q.; Zhou, M. S-doped MIL-53 as efficient heterogeneous electro-Fenton catalyst for degradation of sulfamethazine at circumneutral pH. *J. Hazard. Mater.* **2022**, *424*, 127674. [[CrossRef](#)] [[PubMed](#)]
22. Thiam, A.; Lopez-Ruiz, J.A.; Barpaga, D.; Garcia-Segura, S. The Surge of Metal–Organic-Framework (MOFs)-Based Electrodes as Key Elements in Electrochemically Driven Processes for the Environment. *Molecules* **2021**, *26*, 5713. [[CrossRef](#)] [[PubMed](#)]
23. Teo, W.L.; Zhou, W.; Qian, C.; Zhao, Y. Industrializing metal–organic frameworks: Scalable synthetic means and their transformation into functional materials. *Mater. Today* **2021**, *47*, 170–186. [[CrossRef](#)]
24. Castañeda-Ramírez, A.A.; Rojas-García, E.; López-Medina, R.; García-Martínez, D.C.; Nicolás- Antúnez, J.; Maubert-Franco, A.M. Magnetite nanoparticles into Fe-BTC MOF as adsorbent material for the remediation of metal (Cu(II), Pb(II), As(III) and Hg(II)) ions-contaminated water. *Catal. Today* **2022**, *394–396*, 94–102. [[CrossRef](#)]
25. García, E.R.; Medina, R.L.; Lozano, M.M.; Pérez, I.H.; Valero, M.J.; Maubert Franco, A.M. Adsorption of azo-dye Orange II from aqueous solutions using a metal-organic framework material: Iron- benzenetricarboxylate. *Materials* **2014**, *7*, 8037–8057. [[CrossRef](#)] [[PubMed](#)]
26. Thommes, M.; Kaneko, K.; Neimark, A.V.; Olivier, J.P.; Rodriguez-Reinoso, F.; Rouquerol, J.; Sing KS, W. Physisorption of gases, with special reference to the evaluation of surface area and pore size distribution (IUPAC Technical Report). *Pure Appl. Chem.* **2015**, *87*, 1051–1069. [[CrossRef](#)]
27. Dalakoti, S.; Singh, N.; Wamba, H.N.; Kaishyop, J.; Divekar, S.; Arya, A.; Dasgupta, S. Rapid Aqueous Medium Organization of Trimesate Metal–Organic Frameworks of Cu, Fe: Exploring Suitability in Gas Separation. *ACS Appl. Energy Mater.* **2023**, *1*, 3309–3322. [[CrossRef](#)]
28. Hu, X.; Lou, X.; Li, C.; Ning, Y.; Liao, Y.; Chen, Q.; Mananga, E.S.; Shen, M.; Hu, B. Facile synthesis of the Basolite F300-like nanoscale Fe-BTC framework and its lithium storage properties. *RSC Adv.* **2016**, *6*, 114483–114490. [[CrossRef](#)]
29. Ploegmakers, J.; Japip, S.; Nijmeijer, K. Mixed matrix membranes containing MOFs for ethylene/ethane separation Part A: Membrane preparation and characterization. *J. Membr. Sci.* **2013**, *428*, 445–453. [[CrossRef](#)]
30. Sapnik, A.F.; Bechis, I.; Collins, S.M.; Johnstone, D.N.; Divitini, G.; Smith, A.J.; Chater, P.A.; Addicoat, M.A.; Johnson, T.; Keen, D.A.; et al. Mixed hierarchical local structure in a disordered metal–organic framework. *Nat. Commun.* **2021**, *12*, 2062. [[CrossRef](#)]
31. Byeon, A.; Yun, W.C.; Kim, J.M.; Lee, J.W. Recent progress in heteroatom-doped carbon electrocatalysts for the two-electron oxygen reduction reaction. *Chem. Eng. J.* **2023**, *456*, 141042. [[CrossRef](#)]
32. Fortunato, G.V.; Bezerra, L.S.; Cardoso ES, F.; Kronka, M.S.; Santos, A.J.; Greco, A.S.; Júnior JL, R.; Lanza MR, V.; Maia, G. Using Palladium and Gold Palladium Nanoparticles Decorated with Molybdenum Oxide for Versatile Hydrogen Peroxide Electroproduction on Graphene Nanoribbons. *ACS Appl. Mater. Interfaces.* **2022**, *14*, 6777–6793. [[CrossRef](#)] [[PubMed](#)]
33. Kronka, M.S.; Fortunato, G.V.; Mira, L.; dos Santos, A.J.; Lanza, M.R.V. Using Au NPs anchored on ZrO<sub>2</sub>/carbon black toward more efficient H<sub>2</sub>O<sub>2</sub> electrogeneration in flow-by reactor for carbaryl removal in real wastewater. *Chem. Eng. J.* **2023**, *452*, 139598. [[CrossRef](#)]
34. Peng, W.; Liu, J.; Liu, X.; Wang, L.; Yin, L.; Tan, H.; Hou, F.; Liang, J. Facilitating two-electron oxygen reduction with pyrrolic nitrogen sites for electrochemical hydrogen peroxide production. *Nat. Commun.* **2023**, *14*, 4430. [[CrossRef](#)] [[PubMed](#)]
35. Fóti, G. Oxidation of Organics by Intermediates of Water Discharge on IrO<sub>2</sub> and Synthetic Diamond Anodes. *Electrochem. Solid-State Lett.* **1999**, *2*, 228. [[CrossRef](#)]
36. Panizza, M.; Cerisola, G. Direct and mediated anodic oxidation of organic pollutants. *Chem. Rev.* **2009**, *109*, 6541–6569. [[CrossRef](#)] [[PubMed](#)]

37. Oturan, N.; Bo, J.; Trellu, C.; Oturan, M.A. Comparative Performance of Ten Electrodes in Electro-Fenton Process for Removal of Organic Pollutants from Water. *ChemElectroChem* **2021**, *8*, 3294–3303. [[CrossRef](#)]
38. Vernasqui, L.G.; dos Santos, A.J.; Fortunato, G.V.; Kronka, M.S.; Barazorda-Ccahuana, H.L.; Fajardo, A.S.; Ferreira, N.G.; Lanza MR, V. Highly porous seeding-free boron-doped ultrananocrystalline diamond used as high-performance anode for electrochemical removal of carbaryl from water. *Chemosphere* **2022**, *305*, 135497. [[CrossRef](#)]
39. Barazorda-Ccahuana, H.L.; Fajardo, A.S.; dos Santos, A.J.; Lanza MR, V. Decentralized approach toward organic pollutants removal using UV radiation in combination with H<sub>2</sub>O<sub>2</sub>-based electrochemical water technologies. *Chemosphere* **2023**, *342*, 140079. [[CrossRef](#)]
40. Fdez-Sanromán, A.; Pazos, M.; Sanromán, M.A.; Rosales, E. Heterogeneous electro-Fenton system using Fe-MOF as catalyst and electrocatalyst for degradation of pharmaceuticals. *Chemosphere* **2023**, *340*, 139942. [[CrossRef](#)]
41. Ganiyu, S.O.; Zhou, M.; Martínez-Huitle, C.A. Heterogeneous electro-Fenton and photoelectro-Fenton processes: A critical review of fundamental principles and application for water/wastewater treatment. *Appl. Catal. B Environ.* **2018**, *235*, 103–129. [[CrossRef](#)]
42. dos Santos, A.J.; Sirés, I.; Alves AP, M.; Martínez-Huitle, C.A.; Brillas, E. Vermiculite as heterogeneous catalyst in electrochemical Fenton-based processes: Application to the oxidation of Ponceau SS dye. *Chemosphere* **2020**, *240*, 124838. [[CrossRef](#)] [[PubMed](#)]
43. Zuo, K.; Garcia-Segura, S.; Cerrón-Calle, G.A.; Chen, F.-Y.; Tian, X.; Wang, X.; Huang, X.; Wang, H.; Alvarez, P.J.J.; Lou, J.; et al. Electrified water treatment: Fundamentals and roles of electrode materials. *Nat. Rev. Mater.* **2023**, *8*, 472–490. [[CrossRef](#)]
44. Tang, S.; Zhao, M.; Yuan, D.; Li, X.; Wang, Z.; Zhang, X.; Jiao, T.; Ke, J. Fe<sub>3</sub>O<sub>4</sub> nanoparticles three-dimensional electro-peroxydisulfate for improving tetracycline degradation. *Chemosphere* **2021**, *268*, 129315. [[CrossRef](#)] [[PubMed](#)]
45. Muzenda, C.; Nkwachukwu, O.V.; Arotiba, O.A. Synthetic Ilmenite (FeTiO<sub>3</sub>) Nanoparticles as a Heterogeneous Electro-Fenton Catalyst for the Degradation of Tetracycline in Wastewater. *Ind Eng Chem Res* **2022**, *61*, 11417–11428. [[CrossRef](#)]
46. Zhang, J.; Qiu, S.; Feng, H.; Hu, T.; Wu, Y.; Luo, T.; Tang, W.; Wang, D. Efficient degradation of tetracycline using core-shell Fe@Fe<sub>2</sub>O<sub>3</sub>-CeO<sub>2</sub> composite as novel heterogeneous electro-Fenton catalyst. *Chem. Eng. J.* **2022**, *428*, 131403. [[CrossRef](#)]
47. Alizadeh, Z.; Jonoush, Z.A.; Rezaee, A. Three-dimensional electro-Fenton system supplied with a nanocomposite of microbial cellulose/Fe<sub>3</sub>O<sub>4</sub> for effective degradation of tetracycline. *Chemosphere* **2023**, *317*, 137890. [[CrossRef](#)]
48. Barhoumi, N.; Olvera-Vargas, H.; Oturan, N.; Huguenot, D.; Gadri, A.; Ammar, S.; Brillas, E.; Oturan, M.A. Kinetics of oxidative degradation/mineralization pathways of the antibiotic tetracycline by the novel heterogeneous electro-Fenton process with solid catalyst chalcopyrite. *Appl. Catal. B Environ.* **2017**, *209*, 637–647. [[CrossRef](#)]
49. Badagoppam Haroon, K.H.; Bhunia, S.K. Fenton-like Catalysts Based on Graphitic Carbon Nitride Nanosheets Decorated with Fe<sub>3</sub>O<sub>4</sub> Nanoparticles for Removal of Colorless Tetracycline. *ACS Appl. Nano Mater.* **2024**. [[CrossRef](#)]
50. Magdaleno, A.L.; Brillas, E.; Garcia-Segura, S.; dos Santos, A.J. Comparison of electrochemical advanced oxidation processes for the treatment of complex synthetic dye mixtures. *Sep. Purif. Technol.* **2024**, *345*, 127295. [[CrossRef](#)]
51. Atrashkevich, A.; Fajardo, A.S.; Westerhoff, P.; Walker, W.S.; Sánchez-Sánchez, C.A.; Garcia-Segura, S. Overcoming barriers for nitrate electrochemical reduction: By-passing water hardness. *Water Res.* **2022**, *225*, 119118. [[CrossRef](#)] [[PubMed](#)]
52. Moreira, F.C.; Boaventura RA, R.; Brillas, E.; Vilar, V.J.P. Electrochemical advanced oxidation processes: A review on their application to synthetic and real wastewaters. *Appl. Catal. B Environ.* **2017**, *202*, 217–261. [[CrossRef](#)]
53. Sirés, I.; Brillas, E.; Oturan, M.A.; Rodrigo, M.A.; Panizza, M. Electrochemical advanced oxidation processes: Today and tomorrow. A review. *Environ. Sci. Pollut. Res.* **2014**, *21*, 8336–8367. [[CrossRef](#)] [[PubMed](#)]
54. Gopal, G.; Alex, S.A.; Chandrasekaran, N.; Mukherjee, A. A review on tetracycline removal from aqueous systems by advanced treatment techniques. *RSC Adv.* **2020**, *10*, 27081–27095. [[CrossRef](#)]
55. Liao, Q.; Rong, H.; Zhao, M.; Luo, H.; Chu, Z.; Wang, R. Interaction between tetracycline and microorganisms during wastewater treatment: A review. *Sci. Total Environ.* **2021**, *757*, 143981. [[CrossRef](#)]

**Disclaimer/Publisher's Note:** The statements, opinions and data contained in all publications are solely those of the individual author(s) and contributor(s) and not of MDPI and/or the editor(s). MDPI and/or the editor(s) disclaim responsibility for any injury to people or property resulting from any ideas, methods, instructions or products referred to in the content.